

Water Resources Research

RESEARCH ARTICLE

10.1029/2021WR029955

Key Points:

- A stochastic snow model is integrated into a land-surface model to represent snow subgrid variability and its change over time
- This subgrid snow treatment is tested in an offline mode of the land-surface model to demonstrate its effectiveness
- The effects of snow subgrid variability on energy components and skin temperature in land-surface models are quantified

Correspondence to:

S. He,
siwei.he@colorado.edu

Citation:

He, S., Smirnova, T. G., & Benjamin, S. G. (2021). Single-column validation of a snow subgrid parameterization in the Rapid Update Cycle Land-Surface Model (RUC LSM). *Water Resources Research*, 57, e2021WR029955. <https://doi.org/10.1029/2021WR029955>

Received 10 MAR 2021
Accepted 24 JUL 2021

Single-Column Validation of a Snow Subgrid Parameterization in the Rapid Update Cycle Land-Surface Model (RUC LSM)

Siwei He^{1,2} , Tatiana G. Smirnova^{1,2} , and Stanley G. Benjamin² 

¹Cooperative Institute for Research in Environmental Sciences, University of Colorado, Boulder, CO, USA, ²NOAA Global Systems Laboratory, Boulder, CO, USA

Abstract Subgrid variability of snow is important in studying surface-atmosphere interactions as it affects grid-scale processes. However, this dynamic variability is currently not well-represented in most land-surface models (LSMs). A stochastic snow model using the Fokker-Planck Equation (FPE) has been developed specifically for representing subgrid variability of snow. In this study, the FPE snow model was coupled into the Rapid Update Cycle (RUC) LSM, which provides lower boundary conditions for the operational NOAA Rapid Refresh and High-Resolution Rapid Refresh weather prediction systems. This coupled land-surface model with subgrid snow processes is named the RUC-Stochastic Snow (SS) LSM. The performance of RUC-SS LSM and RUC LSM is analyzed in detail in initial offline single-column testing over two 13-km × 13-km grid cells. The results show that RUC-SS LSM has a much better capability in estimating snow cover fraction than RUC LSM, especially during the late part of the snow-melting season. The simulated duration of the partially snow-covered period at the snow-melting stage is extended from a few days with RUC LSM to about one month with the RUC-SS LSM, thus improving prediction of surface energy budget components. For example, the latent and sensible heat fluxes and skin temperature increase gradually in the RUC-SS LSM during the transition from full coverage to snow-free conditions. In contrast, this transition happens too quickly in RUC LSM, and the energy-budget components change too abruptly. The results of RUC-SS demonstrate its capability to account for subgrid variability of snow cover and show that considering subgrid variability of snow in LSMs is important for simulating surface-atmosphere interactions.

1. Introduction

The influences of the land-surface properties on the atmosphere have been demonstrated in a large number of studies with regional and global models. These effects include the predictability of weather, planetary boundary-layer evolution and cloud formation, afternoon convection, and tropical cyclone intensification (Santanello et al., 2018) on time scales from days to weeks. Since land-surface properties are highly heterogeneous across a wide range of spatial-temporal scales, it is still a challenge to fully represent these heterogeneities in modeling (e.g., Blöschl et al., 2019; Clark et al., 2015; Dirmeyer et al., 2018; Fan et al., 2019; Santanello et al., 2019; Trier et al., 2004; Vrese & Hagemann, 2016). This deficiency in land-surface representation causes meteorological biases in weather and climate forecast models (Santanello et al., 2018; Vrese & Hagemann, 2016).

Snow can induce sharp spatial heterogeneity of land-surface properties causing complexity in boundary-layer dynamics and energy-exchange processes. Snow is a crucial component of the land surface, and it can cover a large fraction of the Northern Hemisphere land area seasonally (Krinner et al., 2018). The surface properties with and without snow are completely different since albedo of snow can be more than four times as large as that of soil, and thermal conductivity of snow can be many times smaller than that of soil. These differences lead to the vertical fluxes of latent and sensible heat being completely different over snow-covered versus snow-free surfaces. The spatial variability of snow within a computational grid cell of a numerical model is often referred to as subgrid variability of snow (e.g., He, Ohara, & Miller, 2019; Helbig et al., 2015; Liston, 2004; Skaugen & Weltzien, 2016). It has been well known that subgrid variability of snow has a remarkable impact on atmospheric circulation (e.g., Aas et al., 2016; Meng, 2017; Mott et al., 2015, 2017; Nitta et al., 2014; Younas et al., 2017). For example, the High-Resolution Rapid Refresh

(HRRR) model, a NOAA operational regional weather forecast model (Benjamin et al., 2016), experiences difficulties in simulating surface air temperature in late fall and early spring in the areas with patchy snow. Younas et al. (2017) showed that inclusion of a subgrid-scale snow parameterization, which considers elevation bands and prescribed slope angles on four aspects, into a regional climate model can improve its snowpack and hydrological simulations. Mott et al. (2015) numerically investigated the boundary-layer flow development and associated heat-exchange processes over a gradually decreasing snow cover in spring. Mott et al. (2017) also conducted a field experiment through three entire snow-ablation seasons. Their experimental study gives a clear evidence of the strong influence of land-surface variability on the atmospheric boundary-layer flow and the heat exchange over snow. Land-surface models (LSMs) developed to supply accurate lower-boundary conditions to atmospheric models usually assume snow is uniformly distributed within a grid cell, and they can simulate reasonably well the lower-boundary conditions for grid cells that are fully covered with snow or completely snow-free. However, it is still a challenge to represent grid cells that are partially covered with snow.

Subgrid variability of snow is still not effectively parameterized in LSMs although a number of studies have been conducted on representing subgrid variability of snow. In summary, three approaches are commonly used in current numerical models for representing subgrid variability of snow (e.g., Blöschl & Sivapalan, 1995). The first approach uses parametric probability distributions in representing subgrid variability of Snow-Water Equivalent (SWE) with assumption of spatially uniform snow melt (e.g., Liston, 2004; Luce et al., 1999). However, as mentioned by Essery and Pomeroy (2004) and Clark et al. (2011), the assumption of spatially uniform snow melt is questionable. Also, representativeness of these parametric probability distributions is limited as they cannot represent the dynamic evolution of subgrid variability (e.g., Skaugen & Randen, 2013; Egli & Jonas, 2009; He, Ohara, & Miller, 2019). The second approach uses a depletion curve, a relationship between SWE and snow-covered area, in representing subgrid variability of snow (e.g., Dutra et al., 2010; Essery & Pomeroy, 2004; Niu & Yang, 2007; Sellers et al., 1996; Swenson & Lawrence, 2012; Yang et al., 1997). Although different curves are used in different studies, a problem with most depletion curve methods is that their parameters are not directly computable from observed data and, hence, are much harder to estimate (Clark et al., 2011). The third approach divides a grid cell into tiles with different snow accumulation and ablation processes (e.g., Aas et al., 2016; Newman et al., 2014; Younas et al., 2017). This method may give more accurate representation of ablation processes and the overall SWE distribution in the grid cell. It also has potential for allowing horizontal transfers of energy and water among the tiles. The disadvantages of this method are increased computational costs with high-resolution tiling, as well as necessity for high-resolution input data for each tile, such as meteorological forcing, soil properties, and land-use data.

A physically based stochastic snow model considering subgrid variability of snow has been developed by He and Ohara (2019). The model is named the Fokker-Planck Equation (FPE) subgrid snow model (hereafter, the FPE-snow model), and the mechanism behind this model is different from these previously mentioned approaches. In the FPE-snow model, subgrid variability of snow in each grid cell is represented by a probability density function (PDF) of snow depth or SWE. The main advantage of this model is that the PDF is not static but dynamic in both space and time. It is obtained from the solution of an advection-diffusion equation. This means that the time evolution of the subgrid variability of snow can be simulated through the FPE-snow model. The results of He and Ohara (2019) demonstrated that the FPE-snow model has promising potential in improving the representation of snow subgrid variability in grid cells partially covered with snow. In the framework of the FPE snow model, different physically based methods for considering subgrid variability of snow and calculating snow cover fraction of a grid cell can be incorporated. More details on the FPE-snow model are given in Section 2.

The RUC LSM (Smirnova et al., 2016) is the land-surface component in the operational NOAA Rapid Refresh (RAP) (Benjamin et al., 2016) over its North American domain and in the HRRR (Benjamin et al., 2016; Smith et al., 2008) over its conterminous U.S. (CONUS) and Alaska/Arctic domains. The RUC LSM considers the subgrid variability of snow through separate treatment of snow-covered and snow-free portions of the grid cell. The grid-cell snow fraction is evaluated from an assumed linear depletion curve. The surface energy fluxes are aggregated every time step as the weighted average of fluxes computed over snow-covered and snow-free portions. More details on the RUC LSM will be given in Section 2.

In this study, the FPE-snow model was integrated into the RUC LSM for better representation of the subgrid scale variability of snow and, consequently, for a more accurate and physically based estimate of the snow fraction - A critical parameter in RUC LSM's snow model for grid cells with partial snow cover. An accurate snow cover fraction is the prerequisite condition for properly simulating the boundary-layer flow and surface fluxes. For example, overestimating snow cover fraction leads to a cold bias, while underestimating snow cover fraction leads to a warm bias. Therefore, the objectives of this study are to improve the snow subgrid parameterization in the RUC LSM (applicable also to other LSMS) through including the FPE-snow model and to evaluate the effects of subgrid variability of snow on the simulated energy exchanges between surface and atmosphere. This treatment can lead to improved weather forecasts especially during seasonal snow melting period.

2. Methods

2.1. The FPE Subgrid Snow Model

The FPE subgrid snow model is a stochastic snow model developed by He and Ohara (2019) based on the previous work of Kavvas (2003) and Ohara et al. (2008). The purpose of developing this model is to simulate subgrid variability of snow, a process that is, generally not well-parameterized but definitely needed in gridded earth-system modeling. The core equation of this prognostic model can be written in terms of snow-water equivalent (SWE) as

$$\frac{\partial P}{\partial t} = \frac{\partial(F_t P)}{\partial W} + \frac{\partial^2(D_{iff} P)}{\partial W^2}$$

with

$$\begin{aligned} F_t &= \langle -E(\mathbf{x}, t) - M_r(\mathbf{x}, t) + sn(\mathbf{x}, t) + q(\mathbf{x}, t) \rangle \\ D_{iff} &= \int_0^t \text{cov}\left(q(\mathbf{x}_t, t); q(\mathbf{x}_{t-s}, t-s)\right) ds + \int_0^t \text{cov}\left(M_r(\mathbf{x}_t, t); M_r(\mathbf{x}_{t-s}, t-s)\right) ds, \end{aligned} \quad (1)$$

where P is the probability of SWE, t is time [s], W is SWE [m], F_t and D_{iff} are advection [m/s] and diffusion [m^2/s] coefficients, E is sublimation rate [m/s], M_r is snowmelt rate [m/s], sn is new snowfall rate [m/s], q is snow redistribution rate [m/s], s is time lag, \mathbf{x} is spatial vector, $\langle \rangle$ is ensemble average operator, $\text{cov}(\cdot)$ is covariance operator. Equation 1 is a nonlinear advection-diffusion equation, and solutions of this equation are PDFs of W at different times t . Equation 1 is a general form of the Fokker-Planck equation (Fokker, 1914; Heinz, 2011; Planck, 1917).

Equation 1 is derived from the point-scale mass conservation equation of SWE

$$\frac{dW}{dt} = -E - M_r + sn + q. \quad (2)$$

Briefly, there are two steps to obtain Equation 1 from Equation 2. The first step is upscaling the point-scale SWE conservation equation, Equation 2, into the grid scale, which is a stochastic partial differential equation. The second step is deriving the Fokker-Planck equation, which determines the probability density of SWE, through Van Kampen's Lemma (Kavvas, 2003; Van Kampen, 1976) and ensemble averaging. More details on deriving Equation 1 are described by He and Ohara (2019).

2.2. Diffusion Coefficient

Equation 1 is an advection-diffusion equation of probability density for SWE in the grid cell. In this equation, the advection coefficient is determined by the grid-cell-averaged behaviors, such as sublimation, melting, and snowfall. These variables can be calculated from the general deterministic equations on these processes. The diffusion coefficient of Equation 1 is determined by the stochastic processes, which are the spatial variability of snow redistribution and snow melting. The diffusion coefficient is not easy to estimate, as the characteristics of spatial variability have to be included and such information is difficult to obtain. A feasible way to evaluate the diffusion coefficient is given below. The diffusion coefficient has two parts, snow redistribution and snowmelt, that need to be evaluated separately.

2.2.1. Snow Redistribution

From He and Ohara (2019), the snow redistribution term, meaning the snow non-uniform distribution caused by wind and topography, can be evaluated as

$$\int_0^t \text{cov}\left(q(\mathbf{x}_t, t); q(\mathbf{x}_{t-s}, t-s)\right) ds \approx \left(\frac{\rho_{cv} k_*^2}{\rho_{ms} h_{cv}}\right) \text{var}(\nabla^2 z(\mathbf{x})) \text{var}(u(\mathbf{x})) \quad (3)$$

where ρ_{cv} is density of snow in the control volume [kg/m^3], ρ_{ms} is density of mobile snow [kg/m^3], h_{cv} is thickness of the control volume [m], $\text{var}()$ is a variance operator, ∇^2 is the Laplacian operator, $z(\mathbf{x})$ is ground surface elevation [m], $u(\mathbf{x})$ is wind speed [m/s], and k^* is a velocity-based snow drag coefficient. This equation is derived based on the work of Ohara (2014). Based on this equation, snow redistribution depends on the variance of topographic curvature and wind speed in the grid cell.

2.2.2. Snowmelt

Although He and Ohara (2019) successfully evaluated the contribution of snowmelt to the diffusion coefficient in their study, their method is not sufficiently general and difficult to apply widely. A new method for estimating the contribution of snowmelt to the diffusion coefficient has been developed and is presented in this study. This method is based on the subgrid variability of net solar radiation (He, Smirnova, & Benjamin, 2019), and it can be used for a variety of situations. The energy conservation equation of snowmelt rate can be written as (DeWalle & Rango, 2008)

$$M_r(\mathbf{x}, t) = \frac{\Delta Q_m(\mathbf{x}, t)}{L_f \rho_w B} \quad (4)$$

where ΔQ_m is melt energy [W/m^2], ρ_w is the density of liquid water [kg/m^3], L_f is the latent heat of fusion [$0.334 \times 10^6 \text{ J}/\text{kg}$], and B is thermal quality of the snowpack [0.95–0.97, dimensionless]. The melt energy is generally calculated from the energy-budget equation of the snowpack (DeWalle & Rango, 2008)

$$\Delta Q_m(\mathbf{x}, t) = Q_{ns}(\mathbf{x}, t) + Q_{nl}(\mathbf{x}, t) + Q_h(\mathbf{x}, t) + Q_e(\mathbf{x}, t) + Q_g(\mathbf{x}, t) + Q_i(\mathbf{x}, t) \quad (5)$$

where Q_{ns} is net shortwave radiation [W/m^2], Q_{nl} is net longwave radiation [W/m^2], Q_h is sensible heat flux [W/m^2], Q_e is latent heat flux [W/m^2], Q_g is ground heat flux [W/m^2], and Q_i is change in snowpack internal heat storage [W/m^2]. According to Natural Resources Conservation Service (2009) and other studies (e.g., Boudhar et al., 2016; Neale & Fitzharris, 1997), Q_{ns} and Q_{nl} contribute 60%–90% of the energy budget ΔQ_m . Generally, Q_{nl} is a dominant factor in winter while Q_{ns} dominates during the main melting season in spring. Based on this fact, all terms on the right-hand side of Equation 5, except for Q_{ns} , are ignored in snow melting season for simplicity. By substituting simplified Equation 5 into Equation 4, and then into the diffusion coefficient in Equation 1, we have

$$\int_0^t \text{cov}\left(M_r(\mathbf{x}_t, t); M_r(\mathbf{x}_{t-s}, t-s)\right) ds \approx \int_0^t \text{cov}\left(\frac{Q_{ns}(\mathbf{x}_t, t)}{L_f \rho_w B}; \frac{Q_{ns}(\mathbf{x}_{t-s}, t-s)}{L_f \rho_w B}\right) ds \quad (6)$$

With two assumptions: (a) atmospheric conditions and the sun's location parameters (i.e., elevation and azimuth angle) are homogeneous within the same grid cell, and (b) the spatial correlation of shortwave radiation is weak and can be ignored, Equation 6 can be further simplified as

$$\int_0^t \text{cov}\left(\frac{Q_{ns}(\mathbf{x}_t, t)}{L_f \rho_w B}; \frac{Q_{ns}(\mathbf{x}_{t-s}, t-s)}{L_f \rho_w B}\right) ds \approx \frac{1}{L_f \rho_w B} \text{var}(Q_{ns}) \quad (7)$$

The validity of these two assumptions have been verified by He, Smirnova, and Benjamin (2019). To use Equation 7, the variance of net shortwave radiation incident on the variable subgrid surface within the grid cell has to be known. However, no information on the variance of net shortwave radiation is provided although the grid-cell mean of downward shortwave radiation can be obtained from the meteorological forcing for each grid cell. Therefore, we should find a way to estimate the variance from the given mean.

He, Smirnova, and Benjamin (2019) has proposed such a method to estimate the variance of net shortwave radiation from the given mean using the subgrid topographic information. The equation is written as:

$$\text{var}(Q_{ns}) = Q_{ns}^2 \frac{C_v}{C_m^2}$$

with

$$\begin{aligned} C_m &= \langle A_{1,i} \rangle C_1 + \langle A_{2,i} \rangle C_2 + \langle A_{3,i} \rangle C_3 \\ C_v &= C_1^2 \langle A_{1,i}^2 \rangle + C_2^2 \langle A_{2,i}^2 \rangle + C_3^2 \langle A_{3,i}^2 \rangle + 2C_1 C_2 \langle A'_{1,i} A'_{2,i} \rangle + 2C_1 C_3 \langle A'_{1,i} A'_{3,i} \rangle + 2C_2 C_3 \langle A'_{2,i} A'_{3,i} \rangle \\ C_1 &= \cos(\alpha_s) \sin(\gamma_s), \quad C_2 = \cos(\alpha_s) \cos(\gamma_s), \quad C_3 = \sin(\alpha_s) \\ A_{1,i} &= \sin \beta_i \sin \gamma_i, \quad A_{2,i} = \sin \beta_i \cos \gamma_i, \quad A_{3,i} = \cos \beta_i \\ A'_{1,i} &= A_{1,i} - \langle A_{1,i} \rangle, \quad A'_{2,i} = A_{2,i} - \langle A_{2,i} \rangle, \quad A'_{3,i} = A_{3,i} - \langle A_{3,i} \rangle \end{aligned} \quad (8)$$

where Q_{ns} is grid-cell mean net shortwave radiation [W/m^2], C_m is a subgrid topographic coefficient for grid-cell mean net shortwave radiation, C_v is a subgrid topographic coefficient for grid-cell variance of net shortwave radiation, β_i is the slope of a subgrid topographic element with index i , γ_i is the aspect of a subgrid topographic element with index i (North is zero, and is measured positive to the East), α_s is elevation angle of the Sun, γ_s is azimuth (aspect) angle of the Sun, $\langle \rangle$ is ensemble average operator, and ' denotes fluctuation terms.

In Equation 8, the subgrid topographic related variables, $A_{n,i}$, have three components ($n=1, 2, 3$) that need to be calculated from the subgrid topographic information, and such information can be obtained from high-resolution Digital Elevation Model (DEM) data. These three geometrical components account for topographic effects on downward solar radiation. Each component is a combination of slope and aspect. Specifically, $A_{1,i}$ is the component in the eastern direction, $A_{2,i}$ is the component in the northern direction, and $A_{3,i}$ is the component in the horizontal plane (Sproul, 2007). Equation 8 builds a bridge to connect the high-resolution DEM data and the coarser-resolution model grid cell. This means that the high-resolution topographic information can be accounted for even if the model grid cell is at a coarser resolution. Another important advantage of Equation 8 is that it is not computationally expensive as the subgrid topographic information is pre-processed and treated as a static input.

The equations introduced in Sections 2.2.1 and 2.2.2 are sufficient to calculate the diffusion coefficient in Equation 1. Then, Equation 1 can be solved numerically by the same numerical scheme as implemented in He and Ohara (2019).

2.3. RUC LSM

The RUC LSM was developed initially by Smirnova et al. (1997) to provide accurate lower boundary conditions for the hourly updated NOAA RUC weather model (Benjamin et al., 2004) developed then for short-range aviation and severe weather prediction. Later, the RUC LSM became a land-surface option of the community WRF model (Skamarock et al., 2008, 2019) and applied to the WRF-based RAP and HRRR models. Recently, RUC LSM has also been implemented in the Common Community Physics Package (CCPP, 2020) in the NOAA Unified Forecasting System (UFS) as part of the RAP/HRRR physics suite. A brief summary of the RUC LSM characteristics is given in Table A1 of the Appendix.

Over the years, several improvements have been implemented in its snow and frozen soil processes (Smirnova et al., 2000). Also, the non-linear averaging of emissivity and transpiration parameters, described in Smirnova et al. (2013), has been implemented for more accurate energy budget. To improve predictions of surface fluxes over both snow-covered and snow-free areas, roughness length has been computed as a grid-cell “effective” roughness length following the technique from Mason (1988) (Smirnova et al., 2016). The performance of RUC LSM has been extensively evaluated in off-line experiments, such as Phase 2(d) of the Project for Intercomparison of Land-surface Parametrization Schemes (PILPS-2(d)) (Luo et al., 2003; Slater et al., 2001), Snow Models Intercomparison Project (SnowMIP) (Etchevers et al., 2004), SnowMIP2 (Essery et al., 2009; Rutter et al., 2009), and the Earth System Models (ESM)-SnowMIP (Krinner et al., 2018; Menard

et al., 2020). While RUC LSM intentionally uses simplified parameterizations to avoid excessive sensitivity to multiple uncertain parameters (Smirnova et al., 2016), it has been competitive with other more sophisticated snow parameterizations participating in SnowMIP experiments (e.g., Menard et al., 2020).

However, the latest enhancement of the RUC snow model, which treats separately snow-covered and snow-free portions of the grid cells, needs more accurate definition of snow cover fraction (SCF) since this parameter becomes critical for realistic representation of surface fluxes for partially snow-covered grid cells. The original SCF formulation does not take into account subgrid variabilities of snow and uses a simple linear depletion curve approach:

$$c = \min(1.0, W / W_c) \quad (9)$$

where c is snow cover fraction, W is SWE, and W_c is threshold SWE for fractional snow (currently set to 32 mm). This curve can only represent the partially snow-covered case when SWE of the grid cell is smaller than the constant value of SWE threshold. Such a formulation cannot represent physical processes contributing to the subgrid variability of snow; for example, it does not reflect the differences in the snow cover evolution between flat and mountainous areas, which could lead to substantial errors in surface predictions in the mountains. Another challenge is to predict duration of partially snow-covered period accurately, which is problematic without taking into account subgrid variability of snow melting processes. To address these challenges, integrating a stochastic snow model described in Sections 2.1–2.2 into RUC LSM has been conducted to capture subgrid-scale snow processes and to improve accuracy of estimated snow cover fraction.

2.4. RUC-SS LSM

For a more realistic representation of the snow subgrid variability, the FPE-snow model (Section 2.1) has been coupled into the RUC LSM, and the new merged model is named RUC-Stochastic Snow (SS) LSM.

The main difference of RUC-SS LSM compared to RUC LSM is the algorithm for estimating snow cover fraction: RUC LSM uses the depletion-curve approach (Equation 9) while RUC-SS uses the FPE-snow model to calculate snow cover fraction from the PDF of SWE. The effects of wind, topographic characteristics, and incoming short-wave radiation on snow cover fraction are considered in the SS model, while calculating snowmelt rate, sublimation rate, and density of snow is still done inside the snow model of the RUC LSM (Smirnova et al., 2000, 2016). Each grid cell has its own dynamic PDF of SWE, and it is obtained through solving Equation 1 at every time step. The PDF of SWE is the core state variable of the SS model (Equation 1), and the snow cover fraction, c , is computed from the PDF of SWE as follows:

$$c = 1 - P(W = 0) \quad (10)$$

where $P(W = 0)$ means the probability that SWE is equal to zero.

The grid-area averaged SWE, $E[W]$, is also calculated from the PDF of SWE as

$$E[W] = \sum W_i P(W_i) \quad (11)$$

where W_i is a discretized SWE in numerically solving Equation 1, $P(W_i)$ is the probability for SWE to be equal to W_i . A forecast interval usually consists of upper and lower limits between which the future value is expected to lie with a prescribed probability (Nechval, 2013). The limits are called *prediction bounds*, and the interval is called the *prediction interval*. The SWE lower-prediction bound, W_l , and upper-prediction bound, W_u , with a prescribed probability α , are calculated from the PDF of SWE as follows:

$$\sum_{W_i=0}^{W_l} P(W_i) = (1 - \alpha)/2; \quad \sum_{W_i=0}^{W_u} P(W_i) = (1 + \alpha)/2 \quad (12)$$

The mean and prediction interval of snow depth can be calculated from the mean and prediction interval of SWE, respectively. Because the RUC-SS predicts the variation of SWE over an area, it is impossible to evaluate its ability to represent subgrid variability by verifying its prediction at a single point. Thus, simulations have to be conducted at the grid cell covering a finite area. This is different from the general LSMs, whose skill is generally verified in off-line one-dimensional experiments for the well-instrumented reference sites with zero area. The required meteorological forcing variables and parameters for the RUC-SS

Table 1*A Summary on the Basic Information of the 4 Study Sites*

Site	<i>rme_ex</i>	<i>rme_sh</i>	<i>swa</i>	<i>snb</i>
Location	(116.758W, 43.064N)	(116.754W, 43.066N)	(107.71W, 37.91N)	(107.73W, 37.91N)
Elevation	2,094 m	2,019 m	3,371 m	3,714 m
US state	Idaho	Idaho	Colorado	Colorado
Soil	Silty clay	Silty clay	Loamy sand	Bedrock
Vegetation	Grassland	Grassland	Grassland	Tundra

LSM are the same as for the RUC LSM, although the point-scale meteorological forcing in the RUC-SS LSM is interpreted as the mean for the grid cell. The high-resolution topographic information has to be provided to estimate the variance of net shortwave radiation (Equation 8) that goes into the estimation of the diffusion coefficient in Equation 1. Thus, the RUC-SS LSM computes snow cover fraction by taking into account the effects of physically based stochasticity on the subgrid variability of snow. This method to compute snow fraction is a substantial improvement over the depletion curve method used in the RUC LSM, as will be demonstrated in Section 4.

3. Study Areas and Data

3.1. Study Areas

Three ESM-SnowMIP sites in the US (Krinner et al., 2018), Reynolds Mountain East (*rme*) in Idaho, Senator Beck (*snb*) in Colorado, and Swamp Angel (*swa*) in Colorado, are used to test the performance of the RUC LSM versus RUC-SS LSM. From Reba et al. (2011), we know that there are actually two sites in Reynolds Mountain East within 500 meters of each other: One site is in a sheltered location while another one is exposed; therefore, we refer to these sites as *rme_sh* and *rme_ex* in this study. In total, there are four sites used in this study, and Table 1 is a summary of their basic information.

As mentioned earlier, the FPE-snow model is an upscaled model to represent subgrid variability, and it is necessary to apply RUC-SS LSM in a grid cell covering a finite area to fully test its performance. To fulfill this requirement, two grid cells with 13-km \times 13-km area were configured around the sites in Table 1. Figure 1 shows locations of the two grid cells that include four sites. Grid 1 covers sites *rme_sh* and *rme_ex*, and Grid 2 covers sites *swa* and *snb*. The forest-covered fractions for Grids 1 and 2 are 31% and 32%, respectively, according to the National Land Cover Database (NLCD; Homer et al., 2015).

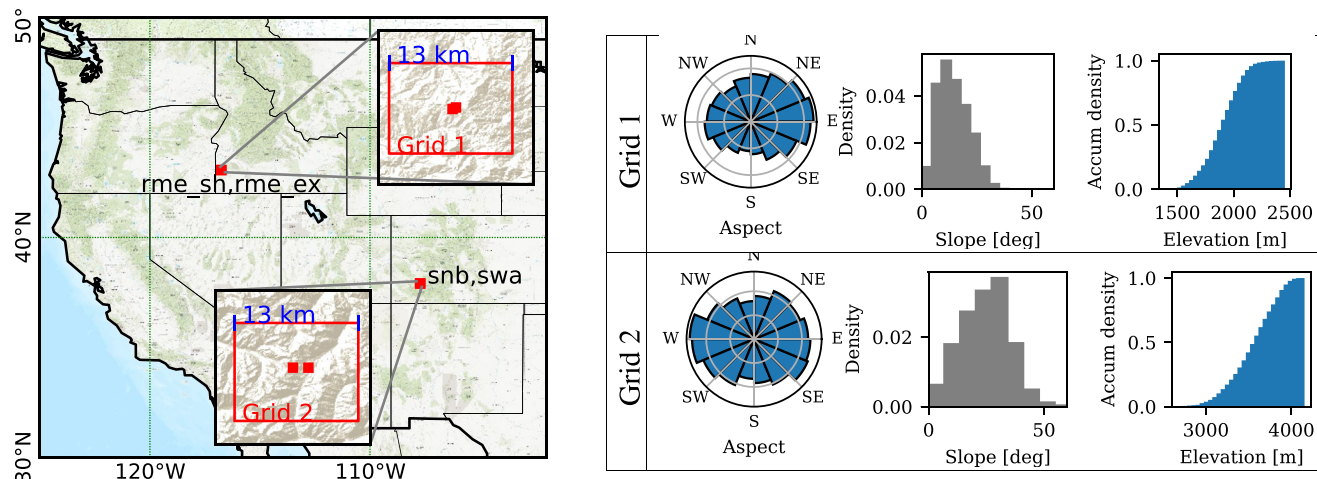


Figure 1. Locations of the two grid cells and four sites. Aspect rose maps, slope histograms, and hypsometric curves of two grid cells are also given on the left.

3.2. Data

Through the ESM-SnowMIP project, three-hourly forcing data have been extracted from the Global Soil Wetness Project Phase 3 (GSWP3) data. The spatial resolution of GSWP3 is 0.5° with a 3-h temporal resolution, and that data were corrected with elevation information for the reference sites and interpolated to hourly time steps (Kriinner et al., 2018) before distribution by the ESM-SnowMIP project. The provided atmospheric variables: surface downward longwave radiation [W/m^2], surface pressure [Pa], 2-m specific humidity [kg/kg], rainfall rate [$\text{kg}/\text{m}^2/\text{s}$], snowfall rate [$\text{kg}/\text{m}^2/\text{s}$], surface downward shortwave radiation [W/m^2], 2-m air temperature [K], and 10-m wind speed [m/s], are used as the meteorological forcing data in this study. In order to estimate subgrid terrain information, 0.333 arc-second Digital Elevation Model (DEM) data are downloaded (<https://www.usgs.gov/core-science-systems/ngp/tnm-delivery/>) and resampled into 50-m resolution for Grids 1 and 2. Then, the required nine topographic variables (variance and covariance in Equation 8) are calculated from the 50-m resolution data for each grid cell.

Two types of validation data are used in this study. The first type of data is point-scale observations, and they are snow depths from site measurements. Point-scale observations only represent the condition at the measured point. If the spatial variability of a variable such as snow depth is large, point-scale observations have a very limited capability in representing the average condition of the grid cell (e.g., Grünwald & Lehning, 2015; Trujillo & Lehning, 2015). The second type of data is grid-scale data, which include remote sensing data and data-assimilation system products. The remote sensing data include snow cover conditions from 30-m spatial resolution Landsat fractional data (Selkowitz & Forster, 2016), 500-m MODIS daily snow cover data (MOD10A1, Hall & Riggs, 2016), and skin temperature from 1-km MODIS daily land surface temperature (LST) data (MOD11A1, Wan, 2014). The products of data assimilation systems include 1-km snow depth and snow cover fraction from SNOW Data Assimilation System (SNODAS) (National Operational Hydrologic Remote Sensing Center, 2004) and 4-km Interactive Multisensor Snow and Ice Mapping System (IMS) Daily Northern Hemisphere Snow and Ice Analysis data (Helfrich et al., 2007; National Snow and Ice Data Center, 2008). The IMS snow and ice data are not ideal for studying the subgrid variability of snow due to the limitation of their spatial resolution, but its daily time resolution is still valuable. Snow cover fraction of $13\text{-km} \times 13\text{-km}$ grid cell is computed from IMS, MODIS, Landsat, and SNODAS data. The temporal resolution of Landsat and MODIS data is 16-day and 1-day, but given missing data for cloudy days, the actual temporal resolution varies with time.

4. Results

4.1. Snow Cover Fraction

The algorithms for calculating snow cover fraction in RUC LSM and RUC-SS LSM are quite different as described above. Again, RUC LSM uses the linear depletion curve while RUC-SS LSM calculates it from the probability density of SWE. Snow cover fraction values from RUC and RUC-SS LSMs were verified against MODIS, Landsat, IMS, and SNODAS data. The results are shown in Figure 2.

Snow cover fraction (SCF) from remote sensing and data assimilation products are not consistent. During the snow accumulation phase in October–November 2005 and 2006, data assimilation products (i.e., IMS and SNODAS) showed more fully snow-covered period than the remote-sensing products (i.e., MODIS and Landsat) in these $13\text{-km} \times 13\text{-km}$ grid cells. Although SCF of IMS and SNODAS are larger than SCF of Landsat and MODIS, consistent snow-cover recessions in the melting season still can be observed from early April to the end of May in Grid 1 and from late April to the end of June in Grid 2. There are several possible explanations for the low values of SCF from MODIS and Landsat including the forest effect on satellite-diagnosed SCF. For example, Wang et al. (2020) mentioned that the algorithm used in MODIS and Landsat in mapping SCF cannot effectively distinguish snow-covered forests from snow-free forests, which may lead to the underestimation of SCF in the forest area.

The most noticeable difference between RUC LSM and RUC-SS LSM occurs in the April–May snow melting period for Grid 1 and May–June snow melting period for Grid 2. For these melting periods, RUC-SS extended the duration of partial snow cover from 2 to 4 days in the original RUC LSM up to more than 50 days, and its decreasing SCF trend during spring is more gradual. For other time periods, the calculated snow cover fractions from RUC LSM and RUC-SS LSM were similar to each other. Comparing against the remote-sensing

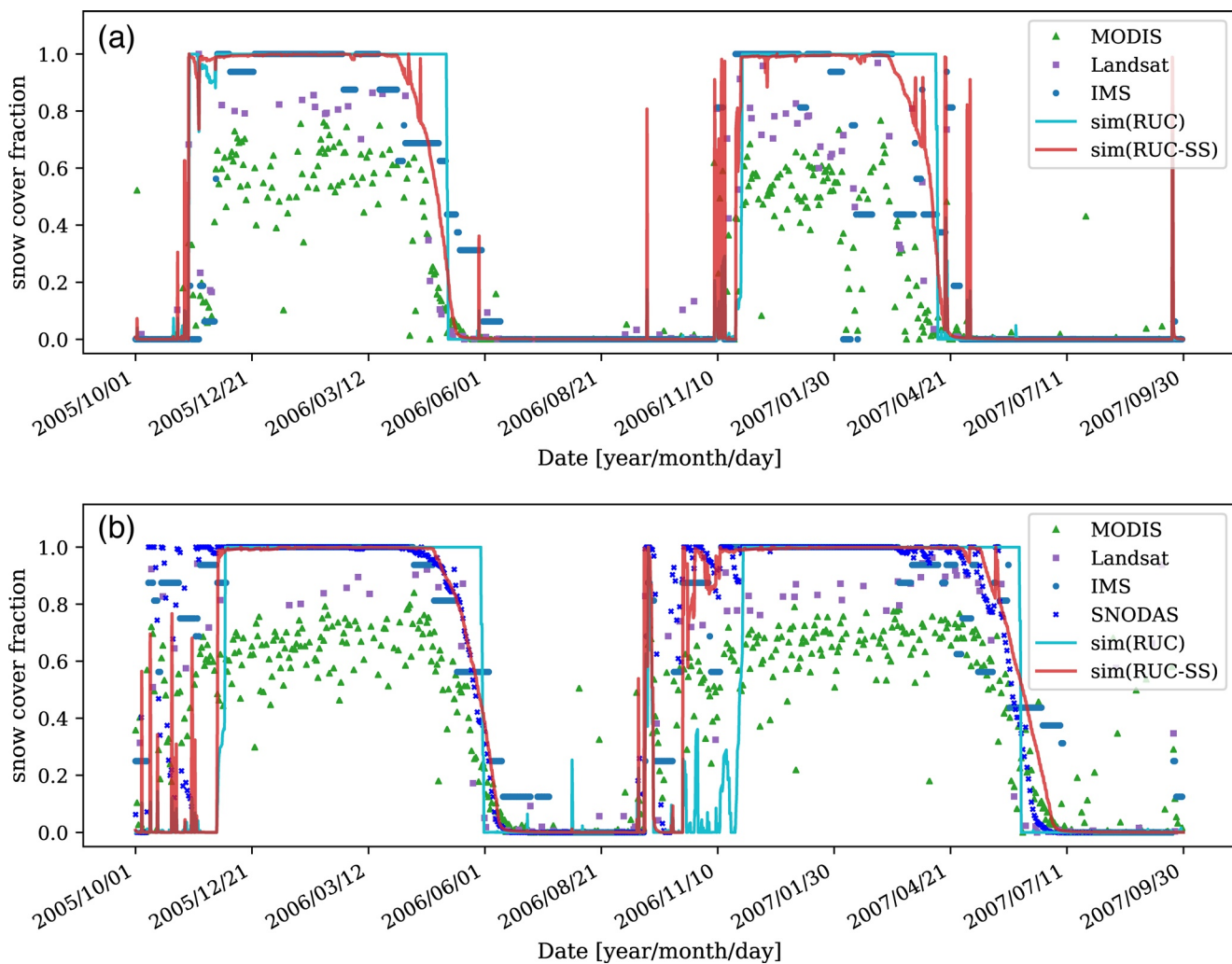


Figure 2. Comparisons of snow cover fractions from Rapid Update Cycle (RUC) and RUC-SS LSMs against MODIS, Landsat, IMS, and SNODAS information. The top panel is for Grid 1 and the bottom panel is for Grid 2.

and data assimilation products, the SCF recession from RUC-SS LSM agreed better with these products in above-mentioned snow melting periods of Grid 1 and Grid 2. RUC-SS agreed especially well with SNODAS and IMS data for Grid 2 in May–June of both years. We found that RUC-SS agreed well with IMS data, but SNODAS SCF values appeared to be much smaller than in RUC-SS and also in other satellite products and in-situ observations in Grid 1. After communicating with SNODAS developing team (Gregory Fall, NOAA), it was discovered that the SNODAS product for Grid 1 was not reliable in year 2005–2007 due to the limitation of the available observation data. Therefore, to avoid confusions, SNODAS data for Grid 1 was not shown in Figure 2.

Finally, we also noted that RUC-SS better captured SCF during the snowfall events both in the early snow accumulation and in the late snow melting periods. In October 2006 for Grid 2, the simulated SCF from RUC-SS reached the maximum of 1.0 after snowfall events while maximum SCF from RUC LSM was around 0.3. Usually during such snowfall events in early snow seasons, the snow accumulates and melts very quickly, and the stochastic snow model demonstrated its ability to capture these processes well. Some abrupt increases of SCF due to snowfall events were also captured by RUC-SS in the snow melting seasons (Figure 2a).

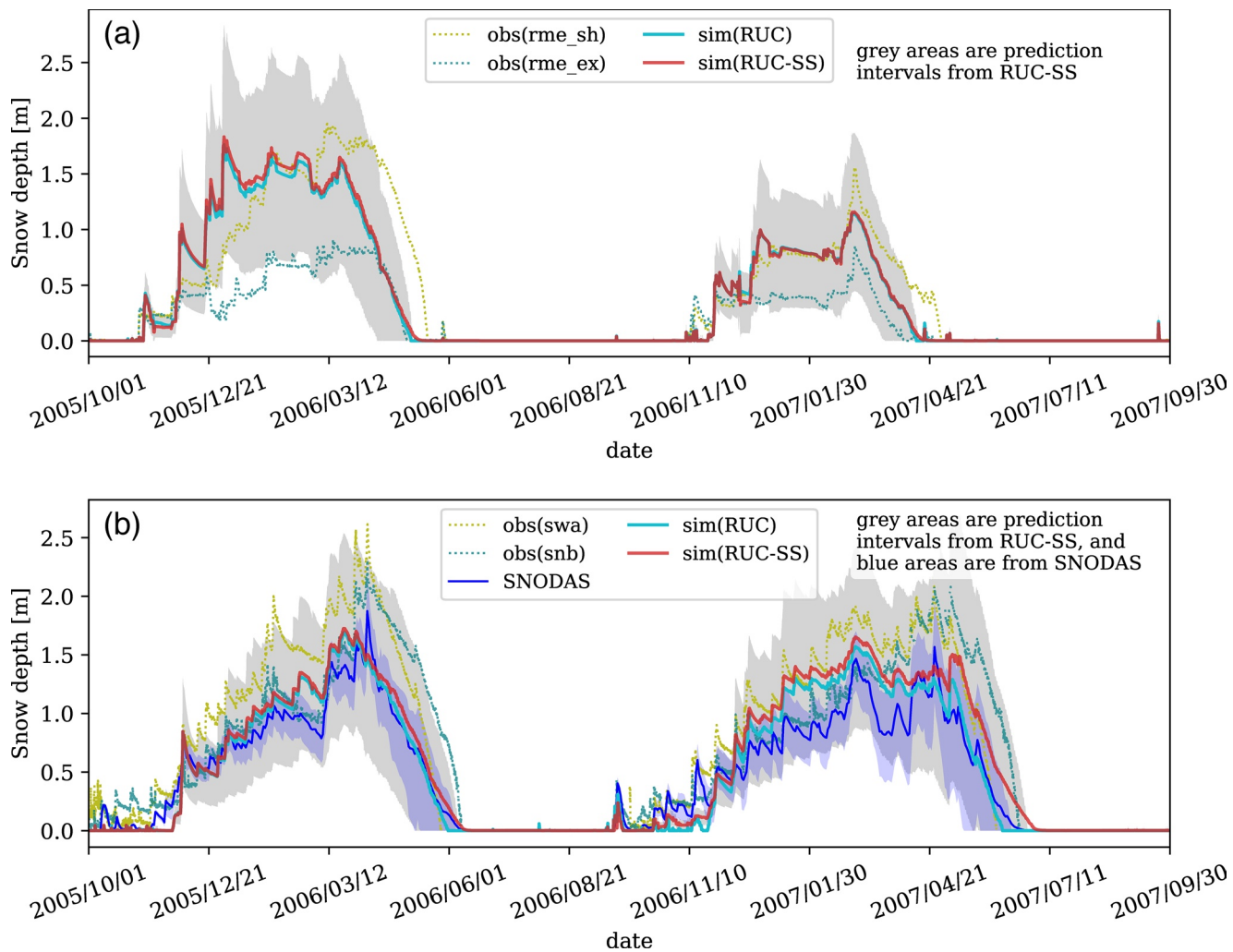


Figure 3. Simulated mean snow depth in Grid 1 (top) and Grid 2 (bottom) compared to the 4 site observations and mean snow depth from SNODAS. Observations are represented in dashed lines, results from RUC LSM are in cyan solid lines, and results from RUC-SS are in red solid lines. The 70% prediction intervals of snow depth from RUC-SS are shown in gray shading, and SNODAS percentiles are given in blue shades.

4.2. Snow Depth

The simulated snow depths from RUC and RUC-SS LSMs are compared to SNODAS data and site observations (Figure 3). Both Grid 1 and Grid 2 include two sites, where snow depth was measured. As mentioned earlier in the description of Equation 12, the FPE-snow model can also estimate the prediction interval of snow depth from the predicted PDF of SWE. The 70% prediction intervals of snow depth from RUC-SS are shown in Figure 3 in gray shading. Since the spatial resolution of SNODAS snow depth is 1 km, a 13-km \times 13-km grid cell includes about 160 SNODAS pixels. Based on these 160 pixels, mean snow depth and 15th and 85th percentiles of snow depth were calculated from SNODAS for Grid 2. The lower and upper boundaries of the areas shaded in blue are from the 15th and 85th percentiles of SNODAS (Figure 3b). As mentioned earlier in the description of Figure 2, SNODAS products for Grid 1 location are not reliable for 2005–2007 and therefore not shown in Figure 3a.

We noted that the observed spatial variability of snow depth was pronounced in these areas. The *in situ* snow depth data showed that the measured snow depth difference between sites *rme_sh* and *rme_ex* within Grid 1 could be up to 1.0 m and the measured snow depth difference between sites *swa* and *snb* within Grid 2 could be up to 0.75 m.

The grid-average snow depth should not be very different either with or without considering subgrid snow variability. The results showed that the maximum difference of the simulated grid-average snow depth between RUC-SS and RUC LSM was less than 0.06 m in Grid 1. The maximum difference was less than 0.1 m in 2006 in Grid 2, but was up to 0.3 m in 2007. Both RUC and RUC-SS LSMs grid-average snow depth matched the SNODAS grid-average snow depth reasonably well in Grid 2, but RUC LSM was even closer to SNODAS than RUC-SS LSM.

We also noted that the simulated 70% prediction intervals of snow depth from RUC-SS LSM covered the *in situ* measurements of Grid 1 and Grid 2 for most of the snow seasons. Exceptions occurred later in snow melting periods. The prediction interval statistically provides information on the possible snow depth within the grid cell. As Figure 3 showed, the range of prediction interval from RUC-SS could be up to 2.0 m, meaning that maximum and minimum snow depths within the grid cells could be up to 2.0 m different. The 15th and 85th percentiles of snow depth from SNODAS were within the prediction interval of the simulated in RUC-SS snow depth for Grid 2.

4.3. Skin Temperature and Surface Fluxes

Subgrid variability of snow affects energy exchange between the surface and the atmosphere. It is essential to investigate how the simulated energy components and skin temperature from RUC-SS are different from RUC LSM for the late snow melting period when the differences between the two models are the largest. The simulated latent and sensible heat fluxes and skin temperature for such period are shown on Figure 4. Also, SCF from RUC and RUC-SS were compared to IMS, MODIS, Landsat, and SNODAS data for the same time. The modeled skin temperatures of Grid 1 and 2 were verified against the mean values of 1-km MODIS Land Surface Temperature (LST) over the 13-km grid cell. The temporal resolution of MODIS LST is about 12 h (for each day, with one daytime value and one nighttime value), so it cannot provide hourly variation of the skin temperature.

These results revealed some positive characteristics of the RUC-SS. First, the simulated SCFs did not match IMS, MODIS, or Landsat exactly; however, SCF from RUC-SS with its gradual decline fitted within the observed range better than SCF from RUC LSM for both Grid 1 and 2.

Second, RUC-SS extended the modeled duration of partial snow cover from 2 to 4 days in RUC LSM to more than 50 days (SCF, Figure 4), and this affects the simulated sensible and latent heat fluxes and the skin temperature. The results (Figure 4) showed that the simulated sensible and latent heat fluxes and skin temperature increased gradually through the melting season in RUC-SS while they increased abruptly within a couple of days in RUC LSM, consistent with the abrupt decrease of SCF from one to zero.

In addition, the snow-depth measurements from the two sites inside Grid 1 and 2 (bottom panels, Figure 4) indicate that the grid cells were partially snow-covered when measured snow depth from one of the two sites was zero while it was non-zero at the second site. This information is an indication of whether the grid cell was partially or fully snow-covered although it only provided a minimum time period for the transition from fully snow-covered to a snow-free condition.

Finally, the MODIS LST data showed that the grid-averaged skin temperature of Grid 1 and 2 (skin T, Figure 4) started to exceed 0°C in the daytime around April 13, 2006 in Grid 1 and April 26, 2007 in Grid 2. For RUC LSM, daytime skin temperature started to exceed 0°C with the delay in time: 21 days delay (around May 4, 2006) in Grid 1 and 42 days delay (June 8, 2007) in Grid 2 due to the overestimated SCF. In contrast, RUC-SS LSM started to have daytime skin temperature above 0°C on time (around April 13, 2006) in Grid 1 and with 12 days delay (around May 26, 2007) in Grid 2. These results showed that RUC-SS LSM captured the variation of the daytime skin temperature better than RUC LSM because of more accurate prediction of SCF. The results of skin temperature also showed that the simulated skin temperature from RUC was warmer than MODIS LST after June 9, 2007 in Grid 2 when RUC LSM melted all snow, but RUC-SS with partial snow cover for this period was slightly colder than MODIS LST.

For the partially snow-covered periods, the simulated energy components and skin temperature highly depend on the accuracy of the simulated snow cover fraction (Figure 4). There could be two scenarios in skin temperature simulations: The first is when cold bias in skin temperature is caused by the overestimated

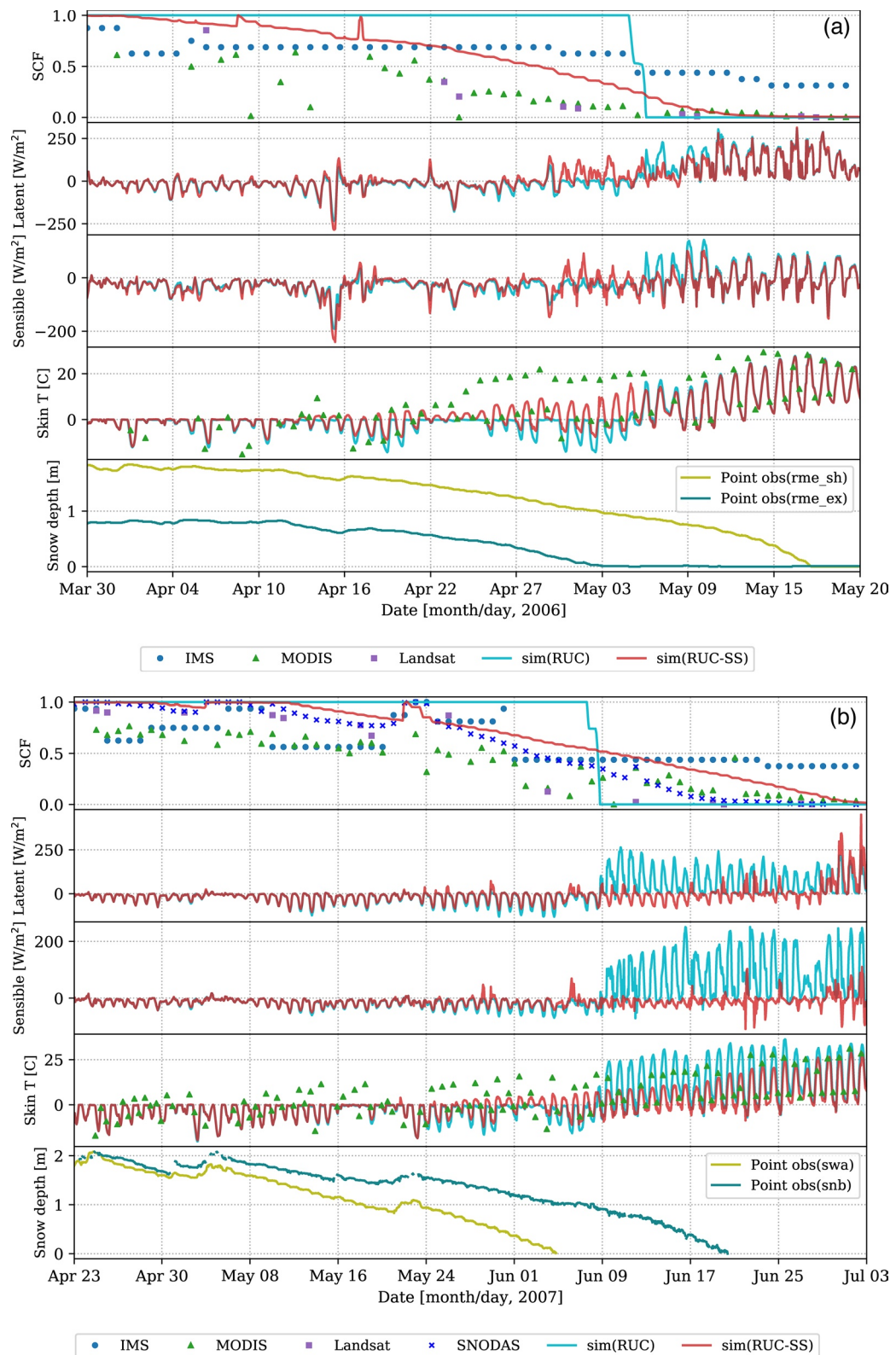


Figure 4. Simulated sensible and latent heat fluxes and skin temperature from the last couple months before the end of a snow season. The top panel is for the Grid 1 in 2006 and the bottom panel is for the Grid 2 in 2007. For each subplot, the variable name is labeled on the vertical axis, and SCF on the top panel represents snow cover fraction.

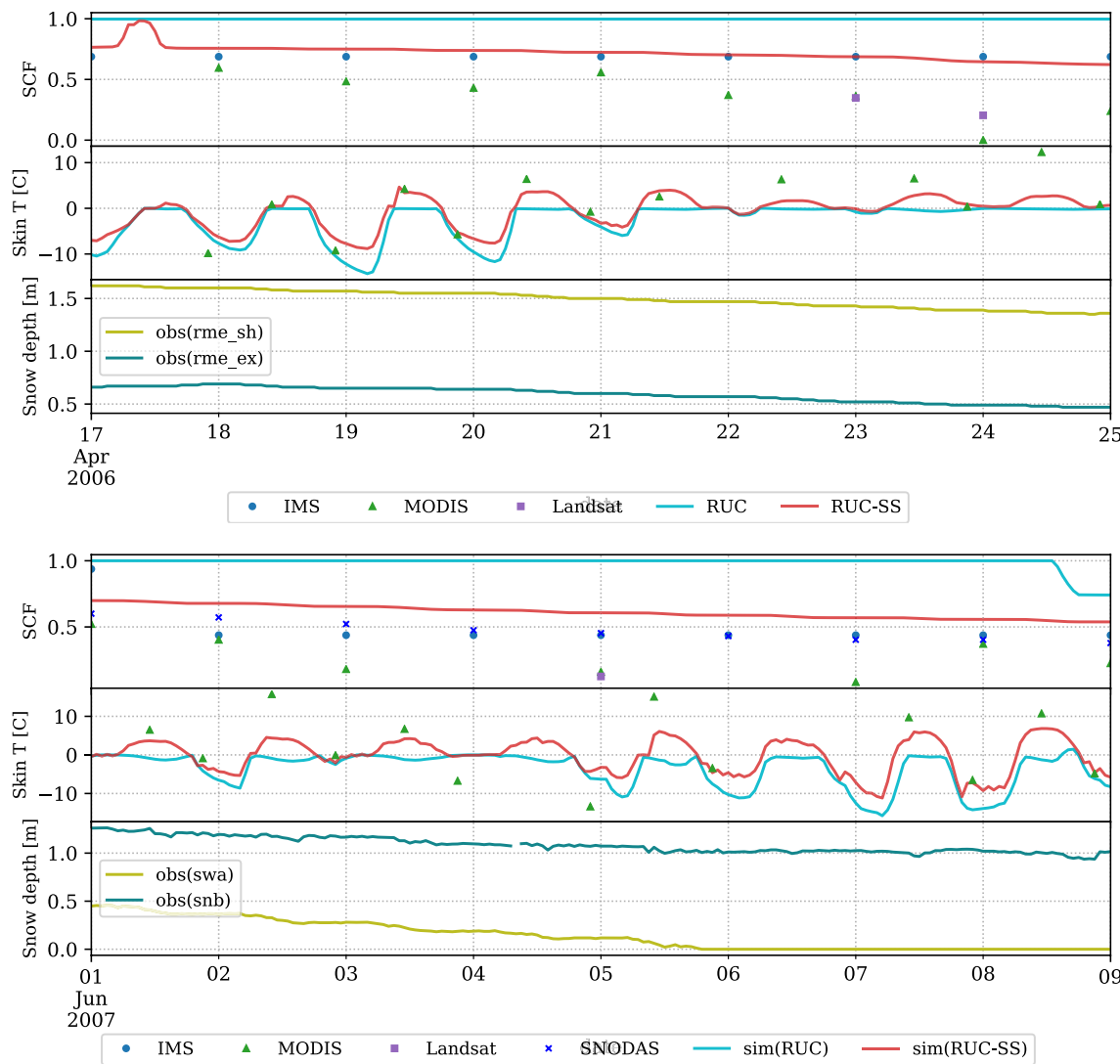


Figure 5. Comparison of the simulated skin temperature against MODIS LST over eight-day long period. SCF and observed snow depth were also included in the plots. The top panel is for April 17–25, 2006 from Grid 1 and the bottom panel is for June 1–9, 2007 from Grid 2. Variables in each subplot are labeled along the vertical axis.

SCF, and the second situation is when warm bias is caused by the underestimation of SCF. The illustration for the first scenario for Grids 1 and 2 is shown in Figure 5.

In Figure 5, MODIS, Landsat, SNODAS, and IMS data showed that the grid cells are partially snow-covered. The performance of RUC-SS was consistent with the remote sensing observations and also had a partial SCF. As a result, the skin temperature from RUC-SS got above 0°C during the day, similar to MODIS LST, while RUC LSM, with grid cells still fully covered with snow, kept daytime skin temperature at 0°C. The mean Root Mean Square Error (RMSE) of the skin temperature from RUC-SS LSM against MODIS LST was 3.7°C in Grid 1 from April 17–25, 2006, and 5.7°C in Grid 2 from June 1–9, 2007. For the same periods, the RMSE of the skin temperature from RUC LSM against MODIS LST was much larger, 5.1°C in Grid 1 and 9.1°C in Grid 2. The averaged cold bias of skin temperature in RUC LSM was reduced from -3.2°C to -1.06°C in RUC-SS in Grid 1 and from -5.7°C to -1.99°C in Grid 2 for this first scenario.

As mentioned earlier, when SCF is underestimated in the model, it may lead to a warm bias. Figure 6 illustrates this second scenario for Grid 2.

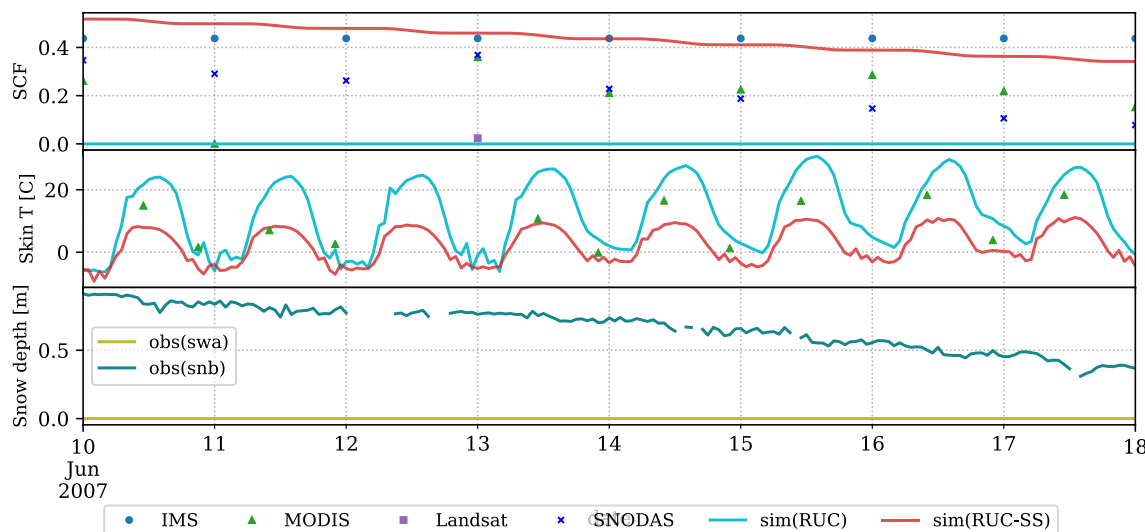


Figure 6. Same as Figure 5, but for 10–18 June 2007 in Grid 2 (Colorado).

MODIS, Landsat, SNODAS, and IMS snow data showed that the Grid 2 is still partially snow-covered for the period shown in Figure 6. Additional support for this partial snow cover diagnosis is that the *snb* site in Grid 2 had snow on the ground while the *swa* site was snow-free. The *snb* site still had snow as it is located in the tundra zone at the elevation 343 m higher than that of the *swa* site. The RUC-SS model is capable to account for such snow depth variability caused by topography, and the top panel of the figure showed that the simulated SCF from RUC-SS was comparable with the observations, while RUC LSM had already melted the entire snowpack in the grid cell. As a result, RUC LSM overestimated skin temperature during this period, and RUC-SS with partial snow cover improved skin temperature simulation. It should be noted that for 5 days out of 8 shown on the figure, daytime skin temperature in RUC-SS was even colder than the MODIS LST. To quantify the improvements in RUC-SS, the mean RMSE and bias of the skin temperature against MODIS LST for June 10–18, 2007 have been computed for both models. The RMSE of skin temperature for RUC LSM is 8.2°C while it is reduced to 6.2°C for RUC-SS LSM. The unrealistic daytime warm bias from RUC LSM was reduced in RUC-SS LSM although it even introduced an undesirable cold bias. The mean bias in RUC LSM was 6.3°C, and –5.4°C in RUC-SS LSM. The statistical verification showed that RUC-SS LSM was capable of taking into account the subgrid snow variability and reduce the RMSEs of skin temperature for this scenario. Further development of RUC-SS LSM is needed to correct cold daytime temperatures.

5. Discussion

In comparisons of predicted RUC and RUC-SS snow cover fraction with IMS, MODIS, Landsat and SNODAS data, RUC-SS LSM better simulates the snowmelt recession limb of SCF than RUC LSM. The simulated duration of the partially snow-covered period from RUC LSM with its depletion-curve approach is underestimated to only 2–4 days for selected melting seasons in two grid cells in Idaho and Colorado, while RUC-SS with its physically based FPE model is capable of extending the simulated duration of partially snow-covered period up to more than 50 days, which is consistent with the observed values from IMS, MODIS, Landsat, and SNODAS for these two grid cells. The improved extension into spring of the partially snow-covered melting period in RUC-SS LSM results from taking into account snow subgrid variability in the stochastic FPE snow model. Based on results for Grid 2 in Colorado, the SCF from RUC-SS matches snow data assimilation product (i.e., SNODAS) better than the satellite-based validation datasets (IMS, MODIS, Landsat). The satellite products generally use a binary snow/non-snow mapping algorithm (SNOMAP) in retrieving snow cover fraction (Hall et al., 1995), which tends to underestimate the amount of snow cover in forest regions (Wang et al., 2020). Both MODIS and Landsat use SNOMAP algorithm, and with 31% and 32% forest fractions for Grids 1 and 2, respectively, the SCF in these regions from MODIS and Landsat are most likely underestimated, but these datasets are still useful to evaluate the SCF trends during snow-melting seasons.

In the RUC-SS LSM, snow depth and SWE of each grid cell are treated as stochastic variables, and they are represented by a dynamic PDF of SWE. The shape of the PDF determines the spatial variability of snow within the grid cell, and the grid-averaged snow depth and SWE in the grid cell can be calculated from the PDF, as illustrated in Equation 11. In contrast, snow depth and SWE in RUC LSM are deterministic variables and are calculated from the mass balance directly, and this deterministic approach gives uniform snow depth and SWE for each grid cell. This shortcoming can be overcome by adding a stochastic snow component to the RUC LSM snow model. Satellite snow observations demonstrate that the spatial heterogeneity of snow distribution within the grid cell could be substantial (e.g., Grünwald & Lehning, 2015; Liston, 2004; Helbig et al., 2015; Skaugen & Weltzien, 2016; Trujillo & Lehning, 2015). This study confirms this and shows that it would be more reasonable to treat snow depth and SWE as stochastic rather than deterministic variables. Pronounced heterogeneity of snow distribution results in differences of snowmelt over time and space. The prolonged melting seasons in RUC-SS accounting for snow heterogeneity, can be caused by longer melting in the portions of the grid cell with a deeper layer of snow accumulated on the ground. This is consistent with findings from Winstral and Marks (2002) showing that the melting periods in Reynolds Mountain East, which is a sub-area of Grid 2, can last more than 50 days. Similar results have been shown in Brauchli et al. (2017).

Prediction intervals shown on the RUC-SS snow depth and SWE plots give statistical evaluation of the possible snow amount within a grid cell. Although it is generally considered to be a rule of thumb to use site observations in evaluating snow model's performance. In reality, snow depth and SWE from a land-surface model are grid-cell averages while *in situ* measurements represent samples of snow depth or SWE from within the grid cell. Using prediction intervals from this method provides a more reasonable way to evaluate model's performance using *in situ* measurements.

Although the SNODAS products are not the 'real' observations, they can be used as a reference in this study. Anderson (2011) found that SNODAS underestimates SWE throughout the winter for most of the Dry Creek Experimental Watershed, which is within the Grid 1 of this study. The finding of Anderson (2011) is consistent with our results showing that SNODAS data underestimates SCF compared to MODIS and LANDSAT data in Grid 1 (Figure 4a). After communicating with the SNODAS development team, we concluded that the SNODAS data in Grid 1 are not reliable since the available observation data in that location were very limited. However, Clow et al. (2012) found that SNODAS can well capture the mean snow depth and SWE in the Colorado Rocky Mountains included in Grid 2, although it has a limited capability in capturing variance, especially in the forested areas. This explains why SNODAS data agrees well with SCF and snow depth from RUC-SS LSM in Grid 2, but the 70% prediction interval from SNODAS is smaller than that from RUC-SS LSM. Another reason why SNODAS cannot capture well spatial variability of snow is that its 1-km spatial resolution is too coarse. As the computational capability improves, hyper-resolution simulation will become possible at small regions (e.g., Marsh et al., 2020), and this may provide an improved way to validate snow subgrid parameterization in larger-scale models.

The results of this study demonstrate that RUC-SS and RUC LSM have the largest differences during the partially snow-covered periods when energy budgets of snow-covered and snow-free areas are computed separately and then combined using the value of snow fraction. Thus, the accuracy of SCF is very important during the periods with partial snow cover. The skin temperature composited over snow-covered and snow-free regions can be above 0°C when a large portion of a grid cell is snow-free. Figures 5 and 6 show that a more accurate method in calculating SCF leads to a more accurate simulation of a grid-cell averaged skin temperature. The simulated skin temperature from RUC-SS LSM during the transition period from fully snow-covered to snow-free conditions matches MODIS LST data better than skin temperature from RUC LSM. MODIS LST data may be not ideal when subpixel and sub-daily variabilities are important, but it still could provide valuable information for verifying the grid-averaged values of the simulated skin temperature. MODIS LST shows that grid-averaged skin temperature can be positive during the daytime more than a month before snow is completely melted (Figure 6). This means that the grid-averaged skin temperature should increase gradually during the transition period from fully snow-covered to snow-free conditions, an evolution captured by RUC-SS LSM.

6. Conclusion

In this study, the FPE-snow model, a stochastic subgrid snow model for representing subgrid variability of snow, is coupled into the RUC LSM. The new model is named RUC-SS LSM. In the RUC-SS LSM, the original method of RUC LSM (i.e., linear depletion curve method) for calculating snow cover fraction is replaced with a method physically taking into account snow subgrid variability, the FPE-snow model. In this model, SWE is treated as a stochastic variable and calculated from the PDF of SWE. The PDF of SWE is the solution of the advection-diffusion equation (i.e., Equation 1) derived from a mass conservation of SWE. Performance of RUC and RUC-SS LSM is compared over two 13-km \times 13-km grid cells, each of them including two ESM-SnowMIP sites (Krinner et al., 2018; Menard et al., 2020). The results demonstrate that RUC-SS has a better capability in simulating snow cover fraction than RUC LSM, and this improves their energy and water exchange simulations further. Such improvements will improve performance of numerical weather prediction (NWP) models.

From the results of this study, we can draw some conclusions on the subgrid variability of snow and its effects on the energy and water exchanges simulations in surface-atmosphere interactions:

1. Subgrid variability of snow distribution is substantial for mountainous regions, therefore snow depth and SWE should be treated as stochastic rather than deterministic variables in numerical models. The proposed approach to account for snow subgrid variability improves predictions of SCF and skin temperature.
2. The most noticeable differences between RUC and RUC-SS LSM happen late in the snow-melting period when the grid cell is partially covered with snow. RUC-SS extends the simulated partially snow-covered period from 2 to 4 days up to more than a month by representing variation of snow depth within the grid cell. The RUC-SS gradual SCF decrease during the melting seasons leads to consequent gradual modifications in the simulated surface fluxes and skin temperature, while in RUC LSM the transition from fully snow-covered to fully snow-free surface state happens too abruptly.
3. RUC-SS corrects cold or warm biases of skin temperature from RUC LSM caused by errors in SCF. Using a linear depletion curve method, the simulated partially snow-covered period from RUC LSM is not captured accurately. Thus, RUC LSM may introduce a cold bias in the simulated skin temperature when SCF is overestimated, typical for the early snow melting stage, or a warm bias when SCF is underestimated, typical for the late snow melting stage. RUC-SS LSM, which includes the stochastic FPE-snow model, reduces such biases as its estimate of SCF from the PDF of SWE is more accurate based on shown verification against the remote sensing data.
4. Comparing with RUC LSM, the simulated state variables and energy-balance components from RUC-SS evolve gradually during a snow-melting stage consistent with the gradual change of SCF. In both RUC and RUC-SS LSM, the grid-scale averaged state variables and energy components are calculated based on the weighted average of snow-covered and snow-free fractions of a grid cell. Thus, more accurate snow cover fraction in RUC-SS reduces RMSEs in skin temperature simulations during the periods with partial snow cover.

Although the proposed comprehensive and physically based parameterization scheme for representing subgrid variability of snow in land-surface models shows improvements in surface predictions with partial snow on the ground, it also has several deficiencies. First, the vegetation effects on the variability of snow are not (yet) explicitly included at subgrid scales for NWP-scale models. It is well-known that vegetation affects wind speed, radiation, horizontal snow redistribution, and rain/snow interception and that different vegetation types have different characteristics. However, a method that can include all these effects into the stochastic snow model hasn't been developed yet. Second, the accuracy of the calculated SCF in RUC-SS depends on the numerical scheme in solving the advection-diffusion equation (Equation 1). Although a second-order numerical scheme, the Monotonic Upstream-centered Scheme for Conservation Laws (MUSCL), is adopted in this study, numerical errors may still exist, especially when mean SWE is very small and variance of SWE is large.

In summary, off-line multi-year testing of the RUC-SS LSM with given atmospheric forcing presented in this study has demonstrated its capabilities to adequately capture subgrid variability of snow. In the future, a test in a fully coupled atmospheric model will be conducted by integrating RUC-SS into the NOAA operational

weather prediction systems: RAP, HRRR, and a regional model using the Unified Forecast System (UFS). The subgrid snow treatment applied in RUC-SS is usable also with other LSMs. Fully coupled testing with continuous cycling of surface and snow variables will be used to further evaluate the skill of the RUC-SS LSM and quantify its effects on snow evolution, surface fluxes, and boundary-layer structure.

Appendix

Table A1*A Brief Summary on the Characteristics of the RUC LSM for Different Processes*

Processes	Representation in RUC LSM
Soil	<ul style="list-style-type: none">• 1-D water transport from Richard's equation (Equation 4, Smirnova et al., 1997)• 1-D heat diffusion equation (Equation 1, Smirnova et al., 1997)• Johansen approach for thermal conductivity (Johansen, 1975)• Staggered vertical grid with 9 levels (Smirnova et al., 1997, 2016)• Parameterization of thawing/freezing processes in soil (Smirnova et al., 2000)• Weighted average of all soil types in the grid cell for soil parameters (Smirnova, et al., 2017a)
Vegetation	<ul style="list-style-type: none">• A "one-leaf" concept for the vegetated portion of the grid cell (Equation 20, Smirnova et al., 1997)• Evapotranspiration (Equations. 9, 16, 18, Smirnova et al., 1997)• Surface parameters (emissivity, transpiration parameter, roughness length) as a non-linear weighted average of all vegetation types in the grid cell (Smirnova et al., 2013)• Seasonal variation of roughness length for a cropland category (Smirnova et al., 2013)• Simple irrigation model for a cropland category (Smirnova et al., 2015)• Interception of snowfall by the vegetation canopy (Smirnova et al., 2016)
Snow	<ul style="list-style-type: none">• Snow model with up to 2 snow layers (Smirnova et al., 2000)• Two-iteration implicit energy budget algorithm for snow melting (Smirnova et al., 2016)• Separate treatment of energy budgets of snow-covered and snow-free portions of the grid cell based on snow cover fraction (Smirnova et al., 2016; Smirnova et al., 2017b)• Aggregate surface energy components of snow-covered and snow-free areas every time step (Smirnova et al., 2016)• Time-dependent density of snow pack on the ground (Smirnova et al., 2016)• Time dependent snow albedo (Smirnova et al., 2016)
Surface fluxes	<ul style="list-style-type: none">• Implicit solution of energy and moisture budgets for a layer spanning the ground surface (Equations. 21–22, Smirnova et al., 1997)
Precipitation forcing	<ul style="list-style-type: none">• Option to accommodate mixed-phase precipitation forcing (Smirnova et al., 2000)• Variable density of solid phase precipitation depending on the hydrometeor type (Smirnova, Brown, & Benjamin, 2017)
Surface runoff	<ul style="list-style-type: none">• Koren-Schaake runoff scheme accounting for spatial variability of hydrological processes (Schaake et al., 1996)
Sea ice	<ul style="list-style-type: none">• 1-D heat diffusion equation (Equations. 1–5, Smirnova et al., 2016)• Snow processes on top of sea ice is simulated using 2-layer snow model (Smirnova et al., 2016)

Data Availability Statement

Source code of the RUC-SS LSM can be accessed through <https://doi.org/10.5281/zenodo.3825277>. MODIS MOD10A1 data can be accessed through <https://nsidc.org/data/mod10a1>, MODIS MOD11A1 data can be accessed through <https://lpdaac.usgs.gov/products/mod11a1v006/>, Landsat Fractional Snow Covered Area data can be accessed through <https://www.usgs.gov/land-resources/nli/landsat/landsat-fractional-snow-covered-area>, SNODAS data can be accessed through <https://nsidc.org/data/g02158>, and IMS data can be accessed through <https://nsidc.org/data/g02158>.

Acknowledgments

The authors thank Dr. John M. Brown of NOAA GSL for insightful reviews of this manuscript. We are especially grateful for very helpful reviews from 3 anonymous reviewers. This work has been supported under NOAA Research base funding and the National Research Council Research Associateships Program. Tatiana G. Smirnova and Siwei He are supported by funding from NOAA Award Number NA17OAR4320101.

References

Aas, K. S., Gisnås, K., Westermann, S., & Berntsen, T. K. (2016). A tiling approach to represent subgrid snow variability in coupled land surface atmosphere models. *Journal of Hydrometeorology*, 18(1), 49–63. <https://doi.org/10.1175/JHM-D-16-0026.1>

Anderson, B. T. (2011). *Spatial distribution and evolution of a seasonal snowpack in complex terrain: An evaluation of the SNODAS modeling product* (p. 181). Boise State University Theses and Dissertations.

Benjamin, S. G., Dévényi, D., Weygandt, S. S., Brundage, K. J., Brown, J. M., Grell, G. A., et al. (2004). An hourly assimilation–forecast cycle: The RUC. *Monthly Weather Review*, 132(2), 495–518. [https://doi.org/10.1175/1520-0493\(2004\)132<0495:AHACTR>2.0.CO;2](https://doi.org/10.1175/1520-0493(2004)132<0495:AHACTR>2.0.CO;2)

Benjamin, S. G., Weygandt, S. S., Brown, J. M., Hu, M., Alexander, C. R., Smirnova, T. G., et al. (2016). A North American hourly assimilation and model forecast cycle: The rapid refresh. *Monthly Weather Review*, 144(4), 1669–1694. <https://doi.org/10.1175/MWR-D-15-0242.1>

Blöschl, G., Bierkens, M. F. P., Chambel, A., Cudennec, C., Destouni, G., Fiori, A., et al. (2019). Twenty-three Unsolved Problems in Hydrology (UPH) – A community perspective. *Hydrological Sciences Journal*, 1141–1158. <https://doi.org/10.1080/02626667.2019.1620507>

Blöschl, G., & Sivapalan, M. (1995). Scale issues in hydrological modelling: A review. *Hydrological Processes*, 9(3–4), 251–290. <https://doi.org/10.1002/hyp.3360090305>

Boudhar, A., Boulet, G., Hanich, L., Sicart, J. E., & Chehbouni, A. (2016). Energy fluxes and melt rate of a seasonal snow cover in the Moroccan High Atlas. *Hydrological Sciences Journal*, 61(5), 931–943. <https://doi.org/10.1080/02626667.2014.965173>

Brauchli, T., Trujillo, E., Huwald, H., & Lehning, M. (2017). Influence of slope-scale snowmelt on catchment response simulated with the alpine3D model. *Water Resources Research*, 53(12), 10723–10739. <https://doi.org/10.1002/2017WR021278>

Clark, M. P., Fan, Y., Lawrence, D. M., Adam, J. C., Bolster, D., Gochis, D. J., et al. (2015). Improving the representation of hydrologic processes in Earth System Models. *Water Resources Research*, 51(8), 5929–5956. <https://doi.org/10.1002/2015WR017096>

Clark, M. P., Hendrikx, J., Slater, A. G., Kavetski, D., Anderson, B., Cullen, N. J., et al. (2011). Representing spatial variability of snow water equivalent in hydrologic and land-surface models: A review. *Water Resources Research*, 47, W07539. <https://doi.org/10.1029/2011WR010745>

Clow, D. W., Nanus, L., Verdin, K. L., & Schmidt, J. (2012). Evaluation of SNODAS snow depth and snow water equivalent estimates for the Colorado Rocky Mountains, USA. *Hydrological Processes*, 26, 2583–2591. <https://doi.org/10.1002/hyp.9385>

Common Community Physics Package (2020). <https://dcicenter.org/community-code/common-community-physics-package-ccpp>

DeWalle, D. R., & Rango, A. (2008). *Principles of snow hydrology*. Cambridge University Press.

Dirmeyer, P. A., Halder, S., & Bombardi, R. (2018). On the Harvest of Predictability from Land States in a Global Forecast Model. *Journal of Geophysical Research: Atmosphere*, 123(23), 111–113. <https://doi.org/10.1029/2018jd029103>

Dutra, E., Balsamo, G., Viterbo, P., Miranda, P. M. A., Beljaars, A., Schär, C., & Elder, K. (2010). An improved snow scheme for the ECMWF land surface model: Description and offline validation. *Journal of Hydrometeorology*, 11(4), 899–916. <https://doi.org/10.1175/2010JHM1249.1>

Egli, L., & Jonas, T. (2009). Hysteretic dynamics of seasonal snow depth distribution in the Swiss Alps. *Geophysical Research Letters*, 36(2). <https://doi.org/10.1029/2008GL035545>

Essery, R., & Pomeroy, J. (2004). Implications of spatial distributions of snow mass and melt rate for snow-cover depletion: Theoretical considerations. *Annals of Glaciology*, 38(1), 261–265. <https://doi.org/10.3189/172756404781815275>

Essery, R., Rutter, N., Pomeroy, J., Baxter, R., Stähli, M., Gustafsson, D., et al. (2009). SNOWMIP2: An evaluation of forest snow process simulations. *Bulletin of the American Meteorological Society*, 90(8), 1120–1136. <https://doi.org/10.1175/2009BAMS2629.1>

Etchevers, P., Martin, E., Brown, R., Fierz, C., Lejeune, Y., Bazile, E., et al. (2004). Validation of the energy budget of an alpine snowpack simulated by several snow models (Snow MIP project). *Annals of Glaciology*, 38, 150–158. <https://doi.org/10.3189/172756404781814825>

Fan, Y., Clark, M., Lawrence, D. M., Swenson, S., Band, L. E., Brantley, S. L., et al. (2019). Hillslope hydrology in global change research and earth system modeling. *Water Resources Research*, 55(2), 1737–1772. <https://doi.org/10.1029/2018WR023903>

Fokker, A. D. (1914). Die mittlere energie rotierender elektrischer dipole im strahlungsfeld. *Annalen der Physik*, 348(5), 810–820. <https://doi.org/10.1002/andp.19143480507>

Grünewald, T., & Lehning, M. (2015). Are flat-field snow depth measurements representative? A comparison of selected index sites with areal snow depth measurements at the small catchment scale. *Hydrological Processes*, 29(7), 1717–1728. <https://doi.org/10.1002/hyp.10295>

Hall, D. K., & Riggs, G. A. (2016). MODIS/Terra snow cover daily L3 Global 500m SIN Grid, Version 6. [MOD10A1]. Boulder, Colorado USA. NASA national snow and ice data center distributed active archive center. <https://doi.org/10.5067/MODIS/MOD10A1.006>

Hall, D. K., Riggs, G. A., & Salmonson, V. V. (1995). Development of methods for mapping global snow cover using moderate resolution imaging spectroradiometer data. *Remote Sensing of Environment*, 54(2), 127–140. [https://doi.org/10.1016/0034-4257\(95\)00137-P](https://doi.org/10.1016/0034-4257(95)00137-P)

He, S., & Ohara, N. (2019). Modeling subgrid variability of snow depth using the Fokker-Planck equation approach. *Water Resources Research*, 55(4), 3137–3155. <https://doi.org/10.1029/2017WR022017>

He, S., Ohara, N., & Miller, S. N. (2019). Understanding subgrid variability of snow depth at 1-km scale using Lidar measurements. *Hydrological Processes*, 33(11), 1525–1537. <https://doi.org/10.1002/hyp.13415>

He, S., Smirnova, T. G., & Benjamin, S. G. (2019b). A scale-aware parameterization for estimating subgrid variability of downward solar radiation using high-resolution digital elevation model data. *Journal of Geophysical Research: Atmosphere*, 124. <https://doi.org/10.1029/2019JD031563>

Heinz, S. (2011). *Mathematical modeling* (1st ed.). Incorporated: Springer Publishing Company.

Helbig, N., van Herwijnen, A., Magnusson, J., & Jonas, T. (2015). Fractional snow-covered area parameterization over complex topography. *Hydrology and Earth System Sciences*, 19(3), 1339–1351. <https://doi.org/10.5194/hess-19-1339-2015>

Helffrich, S. R., McNamara, D., Ramsay, B. H., Baldwin, T., & Kasheta, T. (2007). Enhancements to, and forthcoming developments in the Interactive Multisensor Snow and Ice Mapping System (IMS). *Hydrological Processes*, 21(12), 1576–1586. <https://doi.org/10.1002/hyp.6720>

Homer, C. G., Dewitz, J. A., Yang, L., Jin, S., Danielson, P., Xian, G., et al. (2015). Completion of the 2011 national land cover database for the conterminous United States—representing a decade of land cover change information. *Photogrammetric Engineering & Remote Sensing*, 81(5), 345–354.

Johansen, O. (1975). *Thermal conductivity of soils (PhD thesis)*. Trondheim University.

Kavvas, M. L. (2003). Nonlinear hydrologic processes: Conservation equations for determining their means and probability distributions. *Journal of Hydrologic Engineering*, 8(2), 44–53. [https://doi.org/10.1061/\(ASCE\)1084-0699\(2003\)8:2\(44\)](https://doi.org/10.1061/(ASCE)1084-0699(2003)8:2(44))

Krinner, G., Derkzen, C., Essery, R., Flanner, M., Hagemann, S., Clark, M., et al. (2018). ESM-SnowMIP: Assessing snow models and quantifying snow-related climate feedbacks. *Geoscientific Model Development*, 11(12), 5027–5049. <https://doi.org/10.5194/gmd-11-5027-2018>

Liston, G. E. (2004). Representing subgrid snow cover heterogeneities in regional and global models. *Journal of Climate*, 17, 1381–1397. [https://doi.org/10.1175/1520-0442\(2004\)017<1381:RSSCHI>2.0.CO;2](https://doi.org/10.1175/1520-0442(2004)017<1381:RSSCHI>2.0.CO;2)

Luce, C. H., Tarboton, D. G., & Cooley, K. R. (1999). Sub-grid parameterization of snow distribution for an energy and mass balance snow cover model. *Hydrological Processes*, 13(12–13), 1921–1933. [https://doi.org/10.1002/\(sici\)1099-1085\(199909\)13:12/13<1921::aid-hyp867>3.0.co;2-s](https://doi.org/10.1002/(sici)1099-1085(199909)13:12/13<1921::aid-hyp867>3.0.co;2-s)

Luo, L., Robock, A., Vinnikov, K. Y., Schlosser, C. A., Slater, A. G., Boone, A., et al. (2003). Effects of frozen soil on soil temperature, spring infiltration, and runoff: Results from the PILPS 2(d) Experiment at Valdai, Russia. *Journal of Hydrometeorology*, 4(2), 334–351. [https://doi.org/10.1175/1525-7541\(2003\)4<334:EOFSOS>2.0.CO;2](https://doi.org/10.1175/1525-7541(2003)4<334:EOFSOS>2.0.CO;2)

Marsh, C. B., Pomeroy, J. W., Spiteri, R. J., & Wheater, H. S. (2020). A finite volume blowing snow model for use with variable resolution meshes. *Water Resources Research*, 56(2), e2019WR025307. <https://doi.org/10.1029/2019wr025307>

Mason, P. J. (1988). The formation of areally-averaged roughness lengths. *Quarterly Journal of the Royal Meteorological Society*, 114, 399–420. <https://doi.org/10.1002/qj.49711448007>

Menard, C. B., Essery, R., Krinner, G., Arduini, G., Bartlett, P., Boone, A., et al. (2020). Scientific and human errors in a snow model inter-comparison. *Bulletin of the American Meteorological Society*, 1–46. <https://doi.org/10.1175/BAMS-D-19-0329.1>

Meng, C. (2017). Quantifying the impacts of snow on surface energy balance through assimilating snow cover fraction and snow depth. *Meteorology and Atmospheric Physics*, 129(5), 529–538. <https://doi.org/10.1007/s00703-016-0486-5>

Mott, R., Daniels, M., & Lehning, M. (2015). Atmospheric flow development and associated changes in turbulent sensible heat flux over a patchy mountain snow cover. *Journal of Hydrometeorology*, 16(3), 1315–1340. <https://doi.org/10.1175/JHM-D-14-0036.1>

Mott, R., Schlägl, S., Dirks, L., & Lehning, M. (2017). Impact of extreme land surface heterogeneity on micrometeorology over spring snow cover. *Journal of Hydrometeorology*, 18(10), 2705–2722. <https://doi.org/10.1175/JHM-D-17-0074.1>

National Operational Hydrologic Remote Sensing Center (2004). Snow Data Assimilation System (SNODAS) Data Products at NSIDC, Version 1. [Snow Depth]. Boulder, Colorado USA. NSIDC: National Snow and Ice Data Center. <https://doi.org/10.7265/N5TB14TC>

National Snow and Ice Data Center (2008). *IMS daily northern Hemisphere snow and ice Analysis at 1 km, 4 km, and 24 km resolutions*. <https://doi.org/10.7265/N52R3PMC>

Natural Resources Conservation Service (2009). National Engineering Handbook. In *Part 630: Hydrology*. United States Department of Agriculture (USDA).

Neale, S. M., & Fitzharris, B. B. (1997). Energy balance and synoptic climatology of a melting snowpack in the Southern Alps, New Zealand. *International Journal of Climatology*, 17(14), 1595–1609. [https://doi.org/10.1002/\(SICI\)1097-0088\(19971130\)17:14<1595::AID-JOC213>3.0.CO;2-7](https://doi.org/10.1002/(SICI)1097-0088(19971130)17:14<1595::AID-JOC213>3.0.CO;2-7)

Nechval, K. N. (2013). Proceedings of the 13th International Conference Reliability and Statistics in Transportation and Communication (RelStat13) (Vol. 28–38). Riga. Constructing optimal prediction intervals for future order statistics.

Newman, A. J., Clark, M. P., Winstral, A., Marks, D., & Seyfried, M. (2014). The use of similarity concepts to represent subgrid variability in land surface models: Case study in a snowmelt-dominated watershed. *Journal of Hydrometeorology*, 15(5), 1717–1738. <https://doi.org/10.1175/JHM-D-13-038.1>

Nitta, T., Yoshimura, K., Takata, K., Oishi, R., Sueyoshi, T., Kanae, S., et al. (2014). Representing variability in subgrid snow cover and snow depth in a global land model: Offline validation. *Journal of Climate*, 27, 3318–3330. <https://doi.org/10.1175/JCLI-D-13-0031.1>

Niu, G.-Y., & Yang, Z.-L. (2007). An observation-based formulation of snow cover fraction and its evaluation over large North American river basins. *Journal of Geophysical Research*, 112(D21). <https://doi.org/10.1029/2007JD008674>

Ohara, N. (2014). A practical formulation of snow surface diffusion by wind for watershed-scale applications. *Water Resources Research*, 50(6), 5074–5089. <https://doi.org/10.1002/2013WR014744>

Ohara, N., Kavvas, M. L., & Chen, Z. Q. (2008). Stochastic upscaling for snow accumulation and melt processes with PDF approach. *Journal of Hydrologic Engineering*, 13(12), 1103–1118. [https://doi.org/10.1061/\(asce\)1084-0699\(2008\)13:12\(1103\)](https://doi.org/10.1061/(asce)1084-0699(2008)13:12(1103)

Planck, M. (1917). *Über einen satz der statistischen dynamik und seine erweiterung in der quantentheorie*. Reimer.

Reba, M. L., Marks, D., Seyfried, M., Winstral, A., Kumar, M., & Flerchinger, G. (2011). A long-term data set for hydrologic modeling in a snow-dominated mountain catchment. *Water Resources Research*, 47(7). <https://doi.org/10.1029/2010WR010030>

Rutter, N., Essery, R., Pomeroy, J., Altimir, N., Andreadis, K., Baker, I., et al. (2009). Evaluation of forest snow processes models (Snow-MIP2). *Journal of Geophysical Research*, 114(D6). <https://doi.org/10.1029/2008JD011063>

Santanello, J. A., Dirmeyer, P. A., Ferguson, C. R., Findell, K. L., Tawfik, A. B., Berg, A., et al. (2018). Land–atmosphere interactions: The LoCo perspective. *Bulletin of the American Meteorological Society*, 99(6), 1253–1272. <https://doi.org/10.1175/BAMS-D-17-0001.1>

Santanello, J. A., Jr., Lawston, P., Kumar, S., & Dennis, E. (2019). Understanding the impacts of soil moisture initial conditions on NWP in the context of land–atmosphere coupling. *Journal of Hydrometeorology*, 20(5), 793–819. <https://doi.org/10.1175/jhm-d-18-0186.1>

Schaake, J. C., Koren, V. I., Duan, Q.-Y., Mitchell, K., & Chen, F. (1996). Simple water balance model for estimating runoff at different spatial and temporal scales. *Journal of Geophysical Research*, 101(D3), 7461–7475. <https://doi.org/10.1029/95JD02892>

Selkowitz, D. J., & Forster, R. R. (2016). Automated mapping of persistent ice and snow cover across the western U.S. with Landsat. *ISPRS Journal of Photogrammetry and Remote Sensing*, 117, 126–140. <https://doi.org/10.1016/j.isprsjprs.2016.04.001>

Sellers, P. J., Randall, D. A., Collatz, G. J., Berry, J. A., Field, C. B., Dazlich, D. A., et al. (1996). A revised land surface parameterization (SiB2) for atmospheric GCMS. Part I: model formulation. *Journal of Climate*, 9(4), 676–705. [https://doi.org/10.1175/1520-0442\(1996\)009<0676:ARLSPF>2.0.CO;2](https://doi.org/10.1175/1520-0442(1996)009<0676:ARLSPF>2.0.CO;2)

Skamarock, W. C., Klemp, J. B., Dudhia, J., Gill, D. O., Barker, D., Duda, M. G., et al. (2008). *A description of the advanced research WRF Version 3 (No. NCAR/TN-475+STR)*. University Corporation for Atmospheric Research. <https://doi.org/10.5065/D68S4MVH>

Skamarock, W. C., Klemp, J. B., Dudhia, J., Gill, D. O., Liu, Z., Berner, J., et al. (2019). *A description of the advanced research WRF model version 4 (No. NCAR/TN-556+STR)*. <https://doi.org/10.5065/1dfh-6p97>

Skaugen, T., & Randen, F. (2013). Modeling the spatial distribution of snow water equivalent, taking into account changes in snow-covered area. *Annals of Glaciology*, 54(62), 305–313. <https://doi.org/10.3189/2013AoG62A162>

Skaugen, T., & Weltzien, I. H. (2016). A model for the spatial distribution of snow water equivalent parameterized from the spatial variability of precipitation. *The Cryosphere*, 10, 1947. <https://doi.org/10.5194/tc-10-1947-2016>

Slater, A. G., Schlosser, C. A., Desborough, C. E., Pitman, A. J., Henderson-Sellers, A., Robock, A., et al. (2001). The representation of snow in land surface schemes: results from PILPS 2(d). *Journal of Hydrometeorology*, 2(1), 7–25. [https://doi.org/10.1175/1525-7541\(2001\)002<0007:TROSIL>2.0.CO;2](https://doi.org/10.1175/1525-7541(2001)002<0007:TROSIL>2.0.CO;2)

Smirnova, T., Brown, J. M., & Benjamin, S. (2013). Recent RUC land-surface model enhancements implemented in operational WRF-based Rapid Refresh (RAP). 14th WRF Users' Workshop. <https://www2.mmm.ucar.edu/wrf/users/workshops/WS2013/posters/p91.pdf>

Smirnova, T., Brown, J. M., & Benjamin, S. (2015). *Enhancements in RUC land-surface model implemented in the 3.7 release of the WRF model and land information system*. https://www2.mmm.ucar.edu/wrf/users/workshops/WS2015/short_abstracts/p33.pdf

Smirnova, T., Brown, J. M., & Benjamin, S. (2017b). *Update on land-surface component in operational WRF-based RAP and HRRR*. <https://www2.mmm.ucar.edu/wrf/users/workshops/WS2017/posters/p30.pdf>

Smirnova, T., Brown, J. M., & Benjamin, S. G. (1997). Performance of different soil model configurations in simulating ground surface temperature and surface fluxes. *Monthly Weather Review*, 125(8), 1870–1884. [https://doi.org/10.1175/1520-0493\(1997\)125<1870:PODSMC>2.0.CO;2](https://doi.org/10.1175/1520-0493(1997)125<1870:PODSMC>2.0.CO;2)

Smirnova, T. G., Benjamin, S., & Brown, J. M. M. (2017a). *Memory of cycled land surface stated in RAP and HRRR as a tool to assess the quality of model-data fusion*. 17th Conf. on Hydrology, AMS annual meeting. https://ams.confex.com/ams/97Annual/videogateway.cgi?id=35976&recordingid=35976&uniqueid=Paper303977&entry_password=691193

Smirnova, T. G., Brown, J. M., Benjamin, S. G., & Kenyon, J. S. (2016). Modifications to the rapid update cycle land surface model (RUC LSM) available in the Weather Research and Forecasting (WRF) model. *Monthly Weather Review*, 144(5), 1851–1865. <https://doi.org/10.1175/MWR-D-15-0198.1>

Smirnova, T. G., Brown, J. M., Benjamin, S. G., & Kim, D. (2000). Parameterization of cold-season processes in the MAPS land-surface scheme. *Journal of Geophysical Research*, 105(D3), 4077–4086. <https://doi.org/10.1029/1999JD901047>

Smith, T. L., Benjamin, S. G., Brown, J. M., Weygandt, S., Smirnova, T., & Schwartz, B. (2008). *11.1 Convection forecasts from the hourly updated, 3-km High Resolution Rapid Refresh (HRRR) model*. 24th Conf. on Severe Local Storms. American Meteorological Society. https://ams.confex.com/ams/24SLS/techprogram/paper_142055.htm

Sproul, A. B. (2007). Derivation of the solar geometric relationships using vector analysis. *Renewable Energy*, 32(7), 1187–1205. <https://doi.org/10.1016/j.renene.2006.05.001>

Swenson, S. C., & Lawrence, D. M. (2012). A new fractional snow-covered area parameterization for the Community Land Model and its effect on the surface energy balance. *Journal of Geophysical Research*, (D21), 117. <https://doi.org/10.1029/2012JD018178>

Trier, S. B., Chen, F., & Manning, K. W. (2004). A study of convection initiation in a mesoscale model using high-resolution land surface initial conditions. *Monthly Weather Review*, 132(12), 2954–2976. <https://doi.org/10.1175/mwr2839.1>

Trujillo, E., & Lehning, M. (2015). Theoretical analysis of errors when estimating snow distribution through point measurements. *The Cryosphere*, 9(3), 1249–1264. <https://doi.org/10.5194/tc-9-1249-2015>

Trujillo, E., Ramírez, J. A., & Elder, K. J. (2007). Topographic, meteorologic, and canopy controls on the scaling characteristics of the spatial distribution of snow depth fields. *Water Resources Research*, 43(7), W07409. <https://doi.org/10.1029/2006WR005317>

Van Kampen, N. G. (1976). Stochastic differential equations. *Physics Reports*, 24(3), 171–228. [https://doi.org/10.1016/0370-1573\(76\)90029-6](https://doi.org/10.1016/0370-1573(76)90029-6)

Vrese, P. de, & Hagemann, S. (2016). Explicit representation of spatial subgrid-scale heterogeneity in an ESM. *Journal of Hydrometeorology*, 17(5), 1357–1371. <https://doi.org/10.1175/JHM-D-15-0080.1>

Wan, Z. (2014). New refinements and validation of the collection-6 MODIS land-surface temperature/emissivity product. *Remote Sensing of Environment*, 140, 36–45. <https://doi.org/10.1016/j.rse.2013.08.027>

Wang, X., Chen, S., & Wang, J. (2020). An adaptive snow identification algorithm in the forests of Northeast China. *IEEE Journal of Selected Topics in Applied Earth Observations and Remote Sensing*, 13, 5211–5222. <https://doi.org/10.1109/JSTARS.2020.3020168>

Winstral, A., & Marks, D. (2002). Simulating wind fields and snow redistribution using terrain-based parameters to model snow accumulation and melt over a semi-arid mountain catchment. *Hydrological Processes*, 16(18), 3585–3603. <https://doi.org/10.1002/hyp.1238>

Yang, Z. L., Dickinson, R. E., Robock, A., & Vinnikov, K. Y. (1997). Validation of the snow submodel of the biosphere-atmosphere transfer scheme with Russian snow cover and meteorological observational data. *Journal of Climate*, 10(2), 353–373. [https://doi.org/10.1175/1520-0442\(1997\)010<0353:VOTSSO>2.0.CO;2](https://doi.org/10.1175/1520-0442(1997)010<0353:VOTSSO>2.0.CO;2)

Younas, W., Hay, R. W., MacDonald, M. K., Islam, S. ul, & Déry, S. J. (2017). A strategy to represent impacts of subgrid-scale topography on snow evolution in the Canadian Land Surface Scheme. *Annals of Glaciology*, 58, 1–10. <https://doi.org/10.1017/aog.2017.29>